Unleashing Grid Services Potential of Electric Vehicles for the Volt/VAR Optimization Problem

Arash Farokhi Soofi, *Student Member, IEEE* and Saeed D. Manshadi, *Member, IEEE*

***Abstract*—Emerging utilization of Electric Vehicles (*EV*s) in Distribution Networks (*DN*s) decreases the power quality in the *DN*. The main quest of this research is to find out *Can* EV*s and Photovoltaic (*PV*) systems support the* DN *and mitigate the voltage magnitude violations due to utilizing high penetration level* EV*?* This article proposes a novel volt/VAR optimization (*VVO*) model by leveraging the reactive power support of *EV*s and *PV*s as Distributed Energy Resources (*DER*s) for the *DN*. The proposed *VVO* model contains the second-order conic relaxed form of the *AC* power flow equations. Thus, the presented *VVO* problem is a Mixed-Integer Second-Order Cone Programming (MISOCP) problem. To obtain the ability to support the *DN*, Smart Inverters (*SI*s) are utilized to connect *EV*s and *PV* systems to the *DN*. Thus, to add the *PV* and *EV* systems to the convexified form of the *VVO* problem, the P-Q characteristics and the model of *SI*s working in different operating points are presented based on experimental results. The proposed model of *SI*s allows the participation of *DER*s in the reactive power compensation to mitigate voltage issues of *DN* due to utilizing high penetration level *EV*s. Besides, the proposed model of *SI*s enables *DER*s to increase their dispatchability. The performance of the proposed model is examined in the case studies using the IEEE 33-bus system and 123-bus system. It is illustrated in the case studies that the solar dispatchability increases by 12% when the proposed volt/VAR model is utilized for IEEE 33-bus system. Besides, it is illustrated in the case studies that the voltage profile of buses remains in the desired operating range when the proposed model is leveraged even if the penetration level of *EV*s increased to 40%.**

***Index Terms*—volt/VAR optimization problem, reactive power compensation, smart inverters, *DN* operation, grid services**

NOMENCLATURE

Parameters

α_s^t	Available solar power for solar unit s at time t
B,G	Susceptance and conductance matrices
C_E^t	Cost of electricity at time t
C_D	Degradation cost of the *DER*
C_V	Penalty factor for voltage magnitude violation
$\overline{E}_e$, $\underline{E}_e$	Max./Min. energy level of *EV* fleet e
$\overline{P}_e^d$, $\overline{P}_e^c$	Max. dis/charging power of fleet of *EV* e
p_d^t	Real power demand of load d at time t
$P_{e,t}^{tr}$	Traveling power consumption of *EV* fleet e at time t
q_d^t	Reactive power demand of load d at time t
$\overline{Q}_a^t$	Maximum reactive power of ath quadrant of *SI*
$\underline{Q}_a^t$	Minimum reactive power of ath quadrant of *SI*
R_c^t	The proportion of connected *EV*s at time t
R_{tr}^t	The proportion of traveling *EV*s at time t
$\overline{S}_{ij}$	The maximum apparent power flow of each distribution line
$\overline{V}_i$, $\underline{V}_i$	Voltage magnitude limits of bus i
ρ_a^ζ	Slope of segment ζ of piece-wise linear function of ath quadrant
η_N	The nominal efficiency of *SI* at unity power factor
δ_a^ζ	Maximum reactive power share of segment ζ of quadrant a of the *SI*

Control Variables

$I_e^{ch,t}$	Charging mode status of *EV* e at time t
P_g^t, Q_g^t	Real/Reactive power grid injection at point g into the *DN* at time t
$P_{SI}^{AC,t}$	Real power at the *AC* side of the *SI* at time t
$P_{SI}^{DC,t}$	Real power at the DC side of the *SI* at time t
$P_{e,dc}^{\nu,t}$	V2G DC power of *SI* of *EV* e at time t
$P_{e,t}^{\nu}$	V2G real power at the *AC* side of *SI* of *EV* e at time t
$P_{e,dc}^{c,t}$	Charging DC power of *SI* of *EV* e at time t
$P_{e,t}^{c}$	Charging real power at the *AC* side of *SI* of *EV* e at time t
P_s^t	Real power dispatch of *SI* of solar generation unit s at the *AC* side at time t
$q_a^{\zeta,t}$	Reactive power of segment ζ of ath quadrant of *SI* at time t

State Variables

c, s	lifting operator terms for SOCP relaxation
$\overline{c_i^t}$, $\underline{c_i^t}$	Slack variables representing voltage violation
$E_{e,t}$	Energy of fleet of *EV* e at time t
e_i^t, f_i^t	Real and Imaginary part of voltage phasor of bus i at time t
P_{ij}^t, Q_{ij}^t	Real and reactive power flow between bus i and j at time t
P_Q^t	Real power drop due to reactive power compensation of the *SI* at time t
$\overline{q}_a^{\zeta,t}$	Maximum reactive power of segment ζ of ath quadrant of *SI* at time t
Q_{SI}^t	Reactive power of the *SI* at time t
$Q_{e,t}^{c}$	Charging reactive power exchange between the *SI* of *EV* e and the *DN* at time t
$Q_{e,t}^{\nu}$	V2G reactive power exchange between the *SI* of *EV* e and the *DN* at time t
Q_s^t	Reactive power dispatch of *SI* of solar generation unit s at the *AC* side at time t
V_i	Voltage phasor of bus i

Sets

$\mathcal{BP}$	Set of all buspairs
$\mathcal{BPF}_i$	Set of all buspairs originated from bus i
$\mathcal{E}$	Set of all electric vehicles

Arash Farokhi Soofi is with University of California San Diego, LaJolla, CA, 92093, USA, and San Diego State University, San Diego, CA, 92182 USA. Saeed D. Manshadi is with San Diego State University, San Diego, CA, 92182 USA. e-mail: afarokhi@ucsd.edu; smanshadi@sdsu.edu.

$\mathcal{D}$	Set of all loads
$\mathcal{D}_i$	Set of load connected to bus i
$\mathcal{E}_i$	Set of the electric vehicle connected to bus i
$\mathcal{FB}_{bp}$	Set of the bus which buspair bp originated from
$\mathcal{G}$	Set of all grids connected to the *DN*
$\mathcal{G}_i$	Set of the grid connected to the *DN* through bus i
$\mathcal{I}_e$	Set of the bus connected to *EV* e
$\mathcal{I}_g$	Set of the bus connected to grid g
$\mathcal{I}_l$	Set of the bus connected to load l
$\mathcal{I}_s$	Set of the bus connected to solar generation unit s
$\mathcal{L}$	Set of all branches
$\mathcal{SW}$	Set of all branches with tie switch
$\mathcal{N}$	Set of all buses
$\mathcal{S}$	Set of all solar generation units
$\mathcal{S}_\varsigma$	Set of segments of *SI* ς
$\mathcal{S}_i$	Set of solar generation unit connected to bus i
$\mathcal{T}$	Set of period
$\mathcal{TB}_{bp}$	Set of the bus which buspair bp destined to

I. Introduction

TRANSPORTATION is the second-largest source of global greenhouse gas (GHG) emissions, and it can increase to 60% of the total GHGs emissions by 2050 in the absence of mitigation measures [1]. It is critical to accelerating the adoption of *EV*s, which are now being promoted to replace combustion engine vehicles, in order to reduce GHG emissions from the transportation sector [2]. In [3], the authors presented a smart charging strategy to increase the penetration level of *EV*s and alleviate customer concerns over the limited availability of charging stations. Establishing reliable *EV* charging capabilities from a clean resource is critical to the success of this transition toward *EV* adoption. Thus, the electricity *DN* should be prepared to support the increasing demand of charging *EV*s, where fast charging rate chargers could have an adverse impact on the power quality within the *DN* [4]. In [5], the authors developed the models and methods to evaluate the capacity of electrical energy supply based on voltage stability in the worst charging case scenario and showed the impact of charging location and route choice in the voltage margin limitation. The increasing penetration level of *EV*s will lead to a high electricity demand burden on the power grid especially on the *DN* [6], [7] and decrease the reliability of the *DN* [8]. In [9], authors show the challenges that different *EV* charging methods create for the *DN* operation. In [10], [11], authors investigated the impact of time-of-use pricing and utilizing different methods of charging *EV*s on the voltage magnitude of buses of the *DN*. With the increase of domestic *EV* charging, the existing early evening peak demand will exacerbate [12]. Thus, it is essential to address these challenges of utilizing *EV*s for *DN*s. This paper presents a novel *VVO* method based on the reactive power exchangeability of *SI*s connecting the *EV*s and *PV* systems to the *DN*.

Different methods have been proposed in the literature to mitigate the impact of *EV* charging on the *DN*. One way to mitigate the effect of utilizing high penetration *EV*s on the *DN*s is smart charging [13], [14] Smart charging is defined as the coordinated scheduling of the charging time and charging power of *EV*s [15]. [13] shows that smart charging reduces the percentage of *DN*s that would require reinforcement due to power quality issues originating from deploying high penetration *EV*s. The algorithms proposed to control the *EV* charging varies in the objective, control hierarchy, and the constraints they take into account. Control of *EV* charging is divided into centralized and decentralized methods [16]. In the centralized method, one operator plans the charging schedule of a group of *EV*s. This method provides a structure for *EV* owners to choose their service type based on their average charging need and their willingness to pay to decrease the impact of utilizing high penetration *EV*s on the *DN* [17]. Centralized smart charging schemes are computationally expensive and may not scale to many *EV*s. In the decentralized method, *EV*s control their own charging in response to a signal data input such as electricity price [18], local transformer temperature [19], and the capacity of the local network to prevent overload [20] and stabilizing voltage [21]. The proposed objectives in the literature included: cost minimization [22], peak shaving [23], minimizing losses [24], maximizing compensation of *DER*s [25]. Most methods include an energy constraint, which assures that the SOC of the battery of *EV*s is appropriate. However, some include additional constraints on the network operation [18], battery temperature [26], battery life [27], utilizing long-range *EV*s [28], or voltage and substation capacity limits [22]. However, these centralized and decentralized methods require significant infrastructure to operate, such as centralized or local smart agents, connected and controllable *EV* supply equipment, grid sensors, communication networks, and a scheme to obtain state-of-charge (SOC) data from various *EV* models [29]. Besides, implementing smart charging approaches is very complex and the willingness of the customers is required [15].

Another approach to mitigate the voltage issues of the *DN*s due to deploying high penetration *EV*s is utilizing a home *PV* system integrated with *EV*. In this method, the *EV* battery can mitigate intermittency effects for the home *PV* system [30]. In the noontime, when the electricity demand is less, the excess electric energy from house *PV* systems will be injected into the feeder and can cause voltage rise [31], [32]. Thus, energy storage units are required to mitigate the impact of high penetration house *PV* systems [33], [34]. However, adding batteries to the system cause extra cost and customers might not be willing to invest in energy storage systems. Thus, the utility should invest the money to add energy storage units to prevent solar generation power loss or voltage increase in *DN* [35]. In recent years, researchers proposed the idea to utilize the *EV* battery as an energy storage system where they can store the excess power of *PV* and inject power into the grid when needed [36], [37]. It is studied that the integrated *EV*-*PV* system can provide grid support during the peak demand and mitigates the impacts of high penetration of both residential *PV* systems and *EV*s [38]. However, the *PV* systems generate power only during sunny hours and during this period most *EV*s will be in the workplace instead of home. Thus, most of the solar dispatch would be curtailed during that hours.

An alternative solution to mitigate the impact of utilizing a high penetration level of *EV*s is leveraging *SI*s. *SI*s exchange reactive power with the *DN* to support the *DN* and provide

distribution grid services. Utilizing *SI*s with non-unity power factor by customers decreases the need for voltage management devices implemented by the utility like capacitors and batteries to support the *DN* [39]. Deploying *SI*s can enhance the performance of the *DN* and work as a power factor correction device. Reactive power compensation will allow an increase of *EV* integration with continuous voltage and energy support [40]. The reactive power compensation originates from the real power exchange between the *DER* and the *DN*. Implementing this method enables customers to participate in the grid services. The use of *SI*s for volt/VAR control of high penetration *PV* systems on *DN*s is studied in [41]. In [42], the authors proposed a mixed strategy game between a volt/VAR and Conservation Voltage Reduction optimization model and an optimal energy consumption model to solve the *VVO* problem by considering load shifting, *EV* as the storage and carrier of the energy, and the use of DERs as demand responsive assets. However, this paper does not consider the reactive power support of DERs and its role in *VVO* problem. Most of the papers in the literature have focused on the impact of *EV*s or *PV* systems alone on the *DN*. In [43], authors investigate the impact of *EV* along with *PV* systems on *DN*s with *SI*s. The authors in [44] proposed a multi-objective nonlinear optimal power flow (OPF) problem that can simultaneously improve voltage magnitude and balance profiles while minimizing network losses and generation costs. The proposed *PV* nonlinear operational optimization strategy improves the performance of significantly unbalanced three-phase, four-wire low voltage distribution networks with high residential *PV* penetrations. A bi-level *VVO* approach is presented in [45] where the first level optimizes the control of smart inverters and legacy devices in the network using a linearly approximated method and the second level adjusts the control parameters for smart inverters by solving the approximate OPF model. In [46], the authors presented a two-stage optimization strategy to solve the linearized VVO problem considering high penetration level *EV*s. However, in these studies, the approximate model of *SI*s and the approximate or nonlinear model of the *AC* power flow equations are utilized. Besides, the performance of the *VVO* problem of the *DN* with *SI*s has not been investigated in these studies.

Recent advancements in finding a polynomial-time solution for the optimization problems with *AC* power flow constraints enable the authors of this paper to procure the solution of the *VVO* problem with *AC* power flow constraints. Different relaxation methods including the SOCP relaxation method [47] presented a convex relaxed form of the optimization problem with *AC* power flow constraints with improved relaxation gap. In [48], authors discussed that the SOCP relaxation method is exact for acyclic *DN*s such as *DN*s. Thus in this paper, the solution of the *VVO* problem of *DN*s with *AC* power flow equations and *SI*s connecting the *DER*s to the network is procured by leveraging the SOCP relaxation method. To enable the capability of reactive power compensation of *SI*s, a bidirectional model of *SI*s is presented. The main contributions of this paper are listed as follows:

- Propose a novel *VVO* problem to leverage the potential of *DER*s in compensating the reactive power to increase the power quality of the *DN*s with high penetration level *EV*s.The presented *VVO* problem contains *AC* power flow constraints to investigate the impact of reactive power compensation of *SI*s.
- Model the bidirectional *SI*s operating at different power factors to enable the customers to participate in grid services. The model of *DER*s connected to *SI*s working on different modes is presented and deployed in the proposed volt/VAR method.
- The model of *SI*s based on their operating point is presented to enable *DER*s to support the *DN*s by exchanging reactive power. It is shown that coordinating *SI*s within the *DN* enhances the dispatchability of renewable *DER*s and decreases the unfortunate renewable generation curtailments.

II. Problem Formulation and Solution Methodology

In this section, the reactive power support of *DER*s connected to the *DN* using *SI*s in the volt/VAR optimization problem with *AC* power flow constraints is modeled. First, the exact model of the *SI* based on its operating point and its maximum power is presented. Then, by leveraging the proposed model of *SI*s, the *VVO* problem with *AC* power flow constraints is reformulated using SOCP relaxation in a *DN* with *EV*s and solar generation units working as *DER*s.

A. Smart Inverter's Model

It is supposed that *SI*s are operating in four $P-Q$ quadrants. While Legacy Inverters (LIs) are usually operated in one-way power transfer at the unity power factor, the presented *SI* model exhibits bi-directional power transfer with lower than or equal to the unity power factor. The presented model is consistent with the experimental data presented in [49]. The real power loss of *SI*s changes with the change of the power factor (i.e., the operating point of the *SI*). Each quadrant of the *SI* is divided into $|\mathcal{S}_\varsigma|$ segments. In Fig. 1, the P-Q characteristics of *SI*s are represented with four piece-wised linear functions for each quadrant. The real power of *SI* at the *AC* side at time t depends on the reactive power of the *SI* at time t, the DC power of the *SI* at time t, and the nominal efficiency of the *SI* operating at the unity power factor.

The *SI* works in the first and the second quadrants when the direction of real power flow is from the *DER* to the *DN* as shown in Fig. 2(a). This operating mode of the *SI* is called discharging mode and the piece-wise linear P-Q characteristics of the *SI* are presented in Fig. 1(a). When the *SI* works in quadrants $1, 4$, it dispatches reactive power to the distribution network (i.e., works as a capacitor). This operation mode occurs when the *SI* is compensating for the lack of reactive power to mitigate the voltage magnitude drop. On the contrary, when the *SI* works in quadrants $2, 3$, it works in inductive mode. The real power dispatch of the *SI* in the discharging mode depends on the DC power dispatch of the connected *DER*, the nominal efficiency of the *SI* at the unity power factor, and the real power reduction due to the reactive power support

of the *SI* as presented in (1a). The real power reduction due to the reactive power support of the *SI* depends on the reactive power exchange between the *SI* and the *DN* as presented in (1b). Where the reactive power support of the *SI* is the summation of the reactive power of all segments of the first quadrant minus the summation of the reactive power of all segments of the second quadrant as presented in (1c). It should be noted that the slope of the piece-wised linear functions of the first quadrant is negative, while the one for the second quadrant is positive as shown in Fig. 1(a). The reactive power of segment ζ of the first two quadrants of the *SI* at time t is limited by the maximum reactive power of segment ζ at time t and it is non-negative as presented in (1d). Besides, the reactive power of segments in each quadrant depends on the DC power dispatch of the connected DER, the nominal efficiency of the *SI* at the unity power factor, and the maximum reactive power share of segment ζ of each quadrant of the *SI* (i.e., δ_a^ζ) as presented in (1e). In other words, the reactive power support is always less than or equal to the real power input of the *SI* times the efficiency at the unity power factor. However, there is no limit for the power factor of *SI* and the power factor can vary between 0 and 1. If the *VVO* problem decides the real power input of the *SI* can be increased to increase the reactive power support of each *SI*.

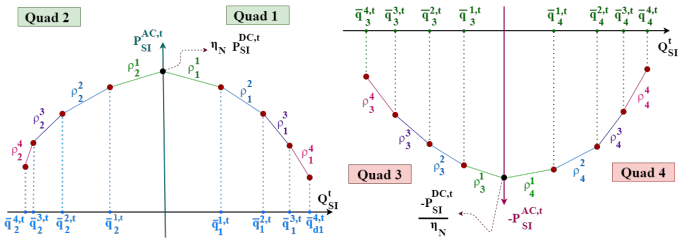

a) Discharging mode of DER b) Charging mode of DER

Fig. 1: The piece-wised linear P-Q characteristics of *SI*s

a) Discharging mode (generation mode) b) Charging mode (load mode)

Fig. 2: The power direction of charging and discharging modes of *SI*s

Decreasing the power factor (i.e., increasing the reactive power compensation of *SI*s) leads to a decrease in the real power of the *SI* as presented in (1a), (1b). Thus, the *SI*'s efficiency decreases with the decrease of the power factor. When the *SI* operates in the first quadrant, the reactive power dispatch of the *SI* is the summation of the reactive power of all segments of the first quadrant of the *SI* as presented in (1c). However, when the *SI* operates in the second quadrant, the reactive power dispatch of the *SI* is the negative of the summation of all reactive power segments of the second quadrant of the *SI* since it is working in inductive mode as presented in (1c).

$$P_{SI}^{AC,t} = \eta_N P_{SI}^{DC,t} - P_Q^t \tag{1a}$$

$$P_Q^t = -\sum_{\zeta\in\mathcal{S}_\zeta} \rho_1^\zeta q_1^{\zeta,t} + \sum_{\zeta\in\mathcal{S}_\zeta} \rho_2^\zeta q_2^{\zeta,t} \tag{1b}$$

$$Q_{SI}^t = \sum_{\zeta\in\mathcal{S}_\zeta} q_1^{\zeta,t} - \sum_{\zeta\in\mathcal{S}_\zeta} q_2^{\zeta,t} \tag{1c}$$

$$0 \le q_a^{\zeta,t} \le \overline{q}_a^{\zeta,t} \qquad : \forall a \in \{1,2\} \tag{1d}$$

$$\text{Where:} \quad \overline{q}_a^{\zeta,t} = \delta_a^\zeta \eta_N P_{SI}^{DC,t} \qquad : \forall a \in \{1,2\} \tag{1e}$$

The *AC* real power of the *SI* in the third and fourth quadrants (i.e., charging mode) depends on the DC power of the *SI*, the efficiency of the *SI* in the unity power factor, and the real power drop due to reactive power support as presented in (2a). However, to provide proper grid services, the *SI* doesn't work in the unity power factor. In this mode, the direction of the real power is from the distribution network toward the *DER* as presented in Fig. 1(b). Thus, the *SI* in the charging mode operates as an inductive (i.e., quadrant 3) or captive (i.e., quadrant 4) load for the *DN* as shown in 2(b). The DC real power drop due to grid services of the *SI* in the charging mode is presented in (2b). Note that the slope of the piece-wise linear functions of the third quadrant is negative, while the one for the fourth quadrant is positive. The total reactive power compensation of the *SI* is the summation of all segments of each quadrant of the *SI* as presented in (2c). The upper and lower limits of the reactive power of segment ζ of the *SI* at time t in charging mode is presented in (2d). Where the reactive power of each segment of the *SI* depends on the real power of the *SI*, the efficiency of the *SI* at unity power factor, and the maximum reactive power share of segment ζ of each quadrant of the *SI* (i.e., δ_a^ζ) as presented in (2e). When the *SI* works in the third quadrant, the total reactive power exchange between the *SI* and the *DN* is the negative of the summation of the reactive power of segments of 3rd quadrant of the *SI* as it is shown in 1(b). In this model, when the *DER* is working in charging mode, it is considered as load and the *AC* real power of its *SI* will appear in the right-hand-side of the nodal balance equation. Thus, the *AC* real power and DC power of *SI*s working in charging mode is non-negative.

$$P_{SI}^{AC,t} = \frac{P_{SI}^{DC,t}}{\eta_N} + P_Q^t \tag{2a}$$

$$P_Q^t = \sum_{\zeta\in\mathcal{S}_\zeta} \rho_4^\zeta q_4^{\zeta,t} - \sum_{\zeta\in\mathcal{S}_\zeta} \rho_3^\zeta q_3^{\zeta,t} \tag{2b}$$

$$Q_{SI}^t = \sum_{\zeta\in\mathcal{S}_\zeta} q_4^{\zeta,t} - \sum_{\zeta\in\mathcal{S}_\zeta} q_3^{\zeta,t} \tag{2c}$$

$$0 \le q_a^{\zeta,t} \le |\overline{q}_a^{\zeta,t}| \qquad : \forall a \in \{3,4\} \tag{2d}$$

$$\text{Where :} \quad |\overline{q}_a^{\zeta,t}| = \delta_a^\zeta |P_{SI}^{AC,t}| \qquad : \forall a \in \{3,4\} \tag{2e}$$

B. Volt/VAR Optimization Problem

In this section, the *VVO* problem of the *DN* with solar generation units and *EV*s connected to the *DN* using *SI*s is presented. The goal of the proposed *VVO* problem is to minimize the operation cost and voltage magnitude violations in distribution networks by utilizing the proposed model of *SI*s.

1) Objective function: The objective function of the *VVO* problem depends on the operation cost of the *DN*, the voltage violation which is penalized, and the degradation cost of *DER*s as presented in (3). The operation cost of the *DN* depends on the time-of-use price of electricity and the real power dispatch of the feeder. Besides, the voltage violation cost depends on the voltage violation at buses of the *DN* and the voltage violation penalty factor. Moreover, the degradation cost of DERs depends on the degradation cost of *EV*s and solar generation units and the dispatch of *EV*s and solar generation units in the *DN*.

$$\min_{P_g^t, P_{e,t}, P_s^t, \underline{c_i^t}, \overline{c_i^t}} \sum_{g\in\mathcal{G}}\sum_{t\in\mathcal{T}} C_E^t P_g^t + \sum_{i\in\mathcal{I}}\sum_{t\in\mathcal{T}} C_V(\underline{c_i^t} + \overline{c_i^t}) + \\ + \sum_{t\in\mathcal{T}}(\sum_{e\in\mathcal{E}} C_D P_{e,t}^{\nu} + \sum_{s\in\mathcal{S}} C_D P_s^t) \tag{3}$$

2) Solar generation units model: The model of solar generation units is presented in (4). The *SI*s connected to solar generation units work in the generation (discharging) mode i.e., first and second quadrants of the P-Q characteristics as shown in Fig. 1(a). It should be noted that in this model for *SI*s, the *AC* real power, DC power, and real power drop due to reactive power support of the *SI* are non-negative. However, the reactive power support of the *SI* can be negative, zero, or positive depending on the reactive power need of the *DN*. The relation between the real power, real power drop due to reactive power support, and the available solar generation power as the power of *SI* in the DC side at time t is presented in (4a). Where the real power drop due to reactive power support of the *SI* depends on the P-Q characteristics of the *SI* and the reactive power of segments of each quadrant of the *SI* connected to solar generation unit s as presented in (4b). Since $P_Q^{s,t}$ and $q_1^{\zeta,t}$ are non-negative and ρ_1^{ζ} is negative, the first term in the right-hand-side (RHS) of (4b) should have negative sign. The total reactive power support of the *SI* of solar s depends on the operating point of the *SI* as presented in (4c). The reactive power of the segment ζ of the *SI* connected to solar s is limited in (4d). The upper limit of the reactive power of segment ζ of the *SI* connected to solar generation unit s at time t depends on the available solar generation power, the efficiency of the *SI* at unity power factor, and share of each segment of each quadrant of the *SI* as shown in (4e). (4f) represents that the DC power of the *SI* connected to solar generation unit s is less than or equal to the available solar power due to the solar generation curtailment capability of *PV* systems.

$$P_s^t = \eta_N P_s^{dc,t} - P_Q^{s,t} \tag{4a}$$

$$P_Q^{s,t} = -\sum_{\zeta\in\mathcal{S}_\varsigma} \rho_1^{\zeta} q_1^{\zeta,t} + \sum_{\zeta\in\mathcal{S}_\varsigma} \rho_2^{\zeta} q_2^{\zeta,t} \tag{4b}$$

$$Q_s^t = \sum_{\zeta\in\mathcal{S}_\varsigma} q_1^{\zeta,t} - \sum_{\zeta\in\mathcal{S}_\varsigma} q_2^{\zeta,t} \tag{4c}$$

$$0 \le q_{s,\zeta}^{a,t} \le \overline{q}_a^{\zeta,t} \qquad : \forall a \in \{1,2\} \tag{4d}$$

$$\text{Where:} \quad \overline{q}_a^{\zeta,t} = \delta_a^{\zeta}\eta_N P_s^{dc,t} \qquad : \forall a \in \{1,2\} \tag{4e}$$

$$0 \le P_s^{dc,t} \le \alpha_s^t \tag{4f}$$

3) EV *model:* The *SI*s connected to *EV*s in V2G mode work in the first and second quadrants i.e. generation mode as shown in Fig. 2(a). However, those connected to *EV*s in charging mode work in the third and fourth quadrants i.e. load mode as shown in Fig. 2(b). The model of the *SI* connected to *EV* e in charging mode is presented in (5). The real power of the *SI* at the *AC* side depends on the DC power of the *SI*, the efficiency of the *SI* at unity PF, and the real power drop due to reactive power support of the *SI* as presented in (5a). Where the real power drop due to reactive power support depends on the reactive power of segments of the *SI* and piece-wised linear function of the P-Q characteristics of the *SI* as presented in (5b). The reactive power of each segment of each quadrant of the *SI* connected to *EV* e at time t is limited in (5d). The upper bound of the reactive power of each segment of each quadrant of the *SI* connected to *EV* e at time t depends on the real power of the *SI* at the *AC* side and the maximum reactive power share of that segment as shown in (5e). As mentioned before, the real power of the *SI* connected to *EV* e at time t working in charging mode is non-negative and its lower bound depends on the proportion of charging *EV*s at time t as presented in (5f). Note that the model of *EV* presented here is a deterministic model, and battery charging time, the charging SOC, a traveling schedule for *EV*s, and other parameters related to the *EV* model are given.

$$P_{e,t}^c = \frac{P_{e,dc}^{c,t}}{\eta_N} + P_{Q,c}^{e,t} \tag{5a}$$

$$P_{Q,c}^{e,t} = \sum_{\zeta\in\mathcal{S}_\varsigma} \rho_4^{\zeta} q_4^{\zeta,t} - \sum_{\zeta\in\mathcal{S}_\varsigma} \rho_3^{\zeta} q_3^{\zeta,t} \tag{5b}$$

$$Q_{e,t}^c = \sum_{\zeta\in\mathcal{S}_\varsigma} q_4^{\zeta,t} - \sum_{\zeta\in\mathcal{S}_\varsigma} q_3^{\zeta,t} \tag{5c}$$

$$0 \le q_{e,a}^{\zeta,t} \le \overline{q}_a^{\zeta,t} \qquad : \forall a \in \{3,4\} \tag{5d}$$

$$\text{Where :} \quad \overline{q}_a^{\zeta,t} = -\delta_a^{\zeta} P_{e,t}^c \qquad : \forall a \in \{3,4\} \tag{5e}$$

$$0 \le P_{e,dc}^{c,t} \le \overline{P}_e^c R_c^t I_e^{ch,t} \tag{5f}$$

The model of *EV*s in V2G mode connected to the *DN* through *SI* is presented in (6). The relation between the real power at the *AC* side of the *SI*, DC power of the *SI*, and the real power drop at the *AC* side of the *SI* due to grid service is presented in (6a). Where the real power drop at the *AC* side of the *SI* due to reactive power compensation is presented in (6b). The relation between the reactive power support of the *SI* and the reactive power of each segment of each quadrant of the *SI* is presented in (6c). Where the upper and lower limit constraints of the reactive power of segment ζ of quadrant a at time t is presented in (6d). The upper limit of the reactive power of segment ζ of quadrant a at time t depends on the DC power of the *SI*, efficiency at unity PF, and maximum reactive power share of segment ζ (6e). The maximum DC power of the *SI* depends on the proportion of charging *EV*s at time t and the maximum charging rate of *EV*s as shown in (6f).

$$P_{e,t}^{\nu} = \eta_N P_{e,dc}^{\nu,t} - P_{Q,\nu}^{e,t} \tag{6a}$$

$$\text{Where:} \quad P^{e,t}_{Q,\nu} = -\sum_{\zeta\in\epsilon}\rho^{\zeta}_1 q^{\zeta,t}_1 + \sum_{\zeta\in\epsilon}\rho^{\zeta}_2 q^{\zeta,t}_2 \tag{6b}$$

$$Q^{\nu}_{e,t} = \sum_{\zeta\in\epsilon} q^{\zeta,t}_1 - \sum_{\zeta\in\epsilon} q^{\zeta,t}_2 \tag{6c}$$

$$0 \le q^{a,t}_{e,\zeta} \le \overline{q}^{\zeta,t}_a \qquad : \forall a \in \{1,2\} \tag{6d}$$

$$\text{Where:} \quad \overline{q}^{\zeta,t}_a = \delta^{\zeta}_a \eta_N P^{\nu,t}_{e,dc} \qquad : \forall a \in \{1,2\} \tag{6e}$$

$$0 \le P^{\nu,t}_{e,dc} \le \overline{P}^{c}_{e} R^{t}_{c}(1 - I^{ch,t}_{e}) \tag{6f}$$

The energy balance of each *EV* fleet at time t is presented in (7a). The physical limits of the energy of *EV* fleet e at time t is presented in (7b).

$$E_{e,t} = E_{e,t-1} - (P^{tr}_{e,t} R^{t}_{tr} + P^{\nu,t}_{e,dc} - P^{c,t}_{e,dc}) \tag{7a}$$

$$\underline{E_e} \le E_{e,t} \le \overline{E_e} \tag{7b}$$

4) Nodal balance and power flow equations: The real and reactive nodal balance at bus i at time t is presented in (8a) and (8b), respectively. The real and reactive power flow on line (i,j) are given in (8c) and (8d), respectively.

$$\sum_{g\in\mathcal{G}_i} P^{t}_{g} + \sum_{s\in\mathcal{S}_i} P^{t}_{s} + \sum_{e\in\mathcal{E}_i} P^{\nu}_{e,t} = \sum_{d\in\mathcal{D}_i} p^{t}_{d} + \sum_{e\in\mathcal{E}_i} P^{c}_{e,t} + (G_{ii} + \sum_{j\in\delta_i} G_{ij})((e^t_i)^2 + (f^t_i)^2) + \sum_{j\in\delta_i} P^{t}_{ij} \tag{8a}$$

$$\sum_{g\in\mathcal{G}_i} Q^{t}_{g} + \sum_{s\in\mathcal{S}_i} Q^{t}_{s} + \sum_{e\in\mathcal{E}_i} Q^{c}_{e,t} + \sum_{e\in\mathcal{E}_i} Q^{\nu}_{e,t} = \sum_{d\in\mathcal{D}_i} q^{t}_{d} - (B_{ii} + \sum_{j\in\delta_i} B_{ij})[(e^t_i)^2 + (f^t_i)^2] + \sum_{j\in\delta_i} Q^{t}_{ij} \tag{8b}$$

$$P^{t}_{ij} = -G_{ij}((e^t_i)^2 + (f^t_i)^2) + G_{ij}(e^t_i e^t_j + f^t_i f^t_j) - B_{ij}(e^t_i f^t_j - e^t_j f^t_i) \tag{8c}$$

$$Q^{t}_{ij} = B_{ij}((e^t_i)^2 + (f^t_i)^2) - B_{ij}(e^t_i e^t_j + f^t_i f^t_j) - G_{ij}(e^t_i f^t_i - e^t_j f^t_i) \tag{8d}$$

Note that equations (8a)-(8d) are presented for single phase full *AC* nodal balance and power flow constraints. These equations have bi-linear terms, which make the *AC VVO* problem a mixed-integer non-convex optimization problem. To relax these bi-linear terms a set of lifting variables is introduced in (9). It should be noted that c^t_{ii} represents the voltage magnitude square of bus i at time t.

$$c^{t}_{ii} := (e^t_i)^2 + (f^t_i)^2; \;\; c^{t}_{ij} := e^t_i e^t_j + f^t_i f^t_j; \;\; s^{t}_{ij} := e^t_j f^t_i - f^t_j e^t_i \tag{9}$$

The SOCP relaxed form of the nodal balance and power flow equations is presented in (10) by leveraging the SOCP lifting variables introduced in (9).

$$\sum_{g\in\mathcal{G}_i} P^{t}_{g} + \sum_{s\in\mathcal{S}_i} P^{t}_{s} + \sum_{e\in\mathcal{E}_i} P^{\nu}_{e,t} = \sum_{d\in\mathcal{D}_i} P^{t}_{d} + \sum_{e\in\mathcal{E}_i} P^{c}_{e,t} + (G_{ii} + \sum_{j\in\delta_i} G_{ij}) c^{t}_{ii} + \sum_{j\in\delta_i} P^{t}_{ij} \tag{10a}$$

$$\sum_{s\in\mathcal{S}_i} Q^{t}_{s} + \sum_{g\in\mathcal{G}_i} Q^{t}_{g} + \sum_{e\in\mathcal{E}_i} Q^{c}_{e,t} + \sum_{e\in\mathcal{E}_i} Q^{\nu}_{e,t} = \sum_{d\in\mathcal{D}_i} q^{t}_{d} - (B_{ii} + \sum_{j\in\delta_i} B_{ij}) c^{t}_{ii} + \sum_{j\in\delta_i} Q^{t}_{ij} \tag{10b}$$

$$P^{t}_{ij} = -G_{ij} c^{t}_{ii} + G_{ij} c^{t}_{ij} + B_{ij} s^{t}_{ij} \tag{10c}$$

$$Q^{t}_{ij} = B_{ij} c^{t}_{ii} - B_{ij} c^{t}_{ij} + G_{ij} s^{t}_{ij} \tag{10d}$$

The relationship between the SOCP lifting variables and the second-order cone relaxation of the relationship between the SOCP lifting terms are presented in (11a) and (11b), respectively.

$$c_{ij} = c_{ji} \quad , \quad s_{ij} = -s_{ji} \tag{11a}$$

$$\left\| \begin{matrix} 2c_{ij} \\ 2s_{ij} \\ c_{ii} - c_{jj} \end{matrix} \right\| \le c_{ii} + c_{jj} \tag{11b}$$

5) Voltage and line limits: Constraint (12a) limits the voltage magnitude of each bus of the *DN* due to the operational limits. The apparent power flow of lines is limited as presented in (12b). Note that the lower and upper voltage magnitude violation squares of bus i at time t are presented as $\overline{c^t_{ii}}, \underline{c^t_{ii}}$ in (12), respectively.

$$\underline{V_i}^2 - \underline{c}^t_i \le (e^t_i)^2 + (f^t_i)^2 \le \overline{V}_i{}^2 + \overline{c}^t_i \tag{12a}$$

$$\sqrt{(P^t_{ij})^2 + (Q^t_{ij})^2} \le \overline{S}_{ij} \tag{12b}$$

The upper limit and lower limit of voltage magnitude at each bus are given in (13), where the SOCP variable corresponding with a squared form of voltage magnitude is leveraged.

$$\underline{V_i}^2 - \underline{c}^t_i \le c^t_{ii} \le \overline{V}_i{}^2 + \overline{c}^t_i \tag{13}$$

The SOCP relaxed form of the *VVO* problem for the *DN* with *EV*s and solar generation units connected through *SI*s to the *DN* is presented in (14). The real power of the *SI* connected to *EV* at time t presented in (5f) and (6f) depends on the *EV* charging binary decision variable (i.e., $I^{ch,t}_e$). Thus, the *VVO* problem in (14) is a MISOCP optimization problem.

$$\begin{aligned} &\text{Objective:} \quad (3) \\ &\text{s.t.} \\ &\underline{c}^t_i, \overline{c}^t_i \ge 0 \\ &(4), (5), (6), (7), (10), (11), (12b), (13) \end{aligned} \tag{14}$$

The *SOCP* relaxation method is tight for acyclic radial networks with cost minimization as the objective function [50]. However, it should be noted that the exactness of the SOCP relaxation is dependent on the network being acyclic and radial, which may not be satisfied in the case of a three-phase unbalanced distribution network. In such cases, the mutual impedance of the three-phase line creates virtual loops in the graph structure, making the network non-radial [51]. However, given that the proposed *VVO* problem in this paper involves a distribution network with a combination of cost minimization and weighted voltage deviation, it can be concluded that the

SOCP relaxation of this problem will produce an exact solution [52]. The SOCP relaxed problem reformulation presented in (14) is exact for radial networks [48]. Since *DN*s are radial, the SOCP relaxation form of the *AC* optimal power flow problem is exact for *DN*s. The presented problem is formulated as a single-level *VVO* problem with MISOCP constraints, solar generation units and *EV*s as *DER*s connected to the *DN* through *SI*s. The structure of the proposed MISOCP *VVO* problem is presented in Fig. 3.

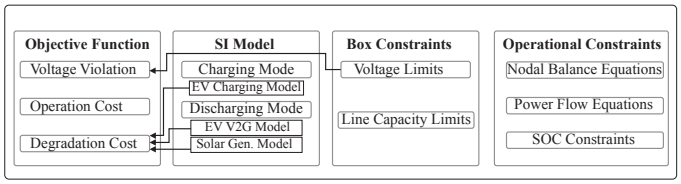

Fig. 3: Visualization of the *VVO* problem

C. Measure of Flat Voltage Magnitude

To evaluate the overall voltage deviation caused by the increasing penetration of *EVs* in the distribution network, we have introduced the Measure of Flat Voltage Magnitude (MFVM) in (15). The *MFVM* indicates the average voltage deviation of the distribution network over a 24-hour period, as illustrated in (15). It is important to note that a distribution network with a MFVM value of zero means that the voltage magnitude of all buses remains within the desired range (i.e., [0.95-1.05] per unit) for the entire 24 hours ($\mathcal{T}$).

$$MFVM = \frac{\sum_{t\in\mathcal{T}}\sum_{i\in\mathcal{I}}(Max\{\left|\sqrt{c_{ii}^{t}}-1\right|,0.05\}-0.05)}{|\mathcal{I}|} \tag{15}$$

III. Case Studies

In this section, two *DN*s are utilized to evaluate the performance of the proposed *VVO* problem. For different networks, the impact of *SI*s on the voltage profile of various buses is investigated. The base demand and solar generation availability are set according to the normalized hourly data of California ISO on August 18, 2020. Here, Gurobi [53] is employed as the off-the-shelf solver to solve the formulated conic programming problem presented in (14). The results presented here are performed on a PC with a Core i7 CPU 4.70GHz processor and 48 GB memory. It should be noted that the negative sign of reactive power of *DER*s (solar generation units and *EV*s) shows the reactive power flow from *DER* to the *DN* and positive reactive power shows the opposite power flow direction. It is worth mentioning that the penetration level of a *DER* in a distribution network is the percentage of houses in the distribution network equipped with that type of DER.

A. Modified IEEE 33-bus system

In this section, the modified IEEE 33-bus *DN* consists of 33 buses, 32 branches, 7 solar generation units, 32 loads, and 32 Electric Vehicle fleets is employed to illustrate the effectiveness of the proposed *VVO* problem and the proposed model for *SI*s. Note that the model of load utilized here is constant power. This type of load is chosen to show the worst-case scenario for the voltage profile of buses throughout the distribution network [10]. The modified IEEE 33-bus system is presented in 4. The impact of utilizing *SI*s on the voltage profile of buses, real power dispatch of the grid connected to the *DN* through the feeder, and the operation cost of the *DN* is investigated in this section. Note that the base net demand and solar generation trends are set according to the normalized hourly data of California ISO on November 4, 2021 [54]. The *VVO* problem is modeled for 24 hours. Thus, it is called one in a day. Therefore, all the results are presented for November 1, 2021.

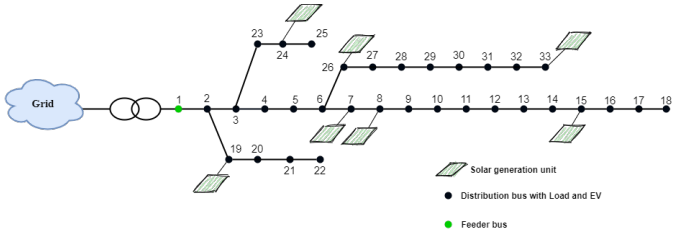

Fig. 4: The modified IEEE 33-bus *DN*

*1) **Impact of utilizing smart inverters on the voltage profile of buses**:* In this section, the voltage profile of buses of the IEEE 33-bus *DN* over 24 hours when Legacy Inverters (LI) are utilized is compared with the one procured by the proposed volt/VAR model with *SI*s. Utilizing *SI*s mitigates the voltage magnitude drop of buses in a *DN* with a high penetration level of *EV*s. Fig. 5 presents the voltage profile of bus 18 over 24 hours procured by the *VVO* problem with different *EV* penetration levels. It should be noted that the farthest bus from the feeder bus, which has the most voltage magnitude violation, is chosen to show how the grid service capability of the *SI*s can mitigate the voltage magnitude violation of buses. When the penetration level of *EV*s is zero, the voltage magnitude of all buses stay within the desired limits of voltage magnitudes (i.e., [0.95-1.05] p.u.). Increasing the penetration level of *EV*s, decreases the voltage magnitudes over all buses. However, the voltage magnitude violation occurs in those buses far from the feeder e.g., buses $15-18$. It is shown in Fig. 5 that deploying *SI*s eradicates this voltage violation. The MFVM index of the *DN* procured by the LI case is 0.075 for a 40% *EV* penetration level, and it is decreased to 0 when the proposed *SI* model is utilized. Besides, the operation cost of the DN procured by the proposed method with *SI* model is decreased 5% to $\$29,775$ compared to the one procured by the *VVO* problem with *LI*s which is $\$31,324$. It should be noted that the solution time of the proposed model is 374 seconds for the IEEE 33-bus system.

Fig. 6 illustrates how the *SI*s serve the grid by dispatching the reactive power to maintain the voltage magnitudes in

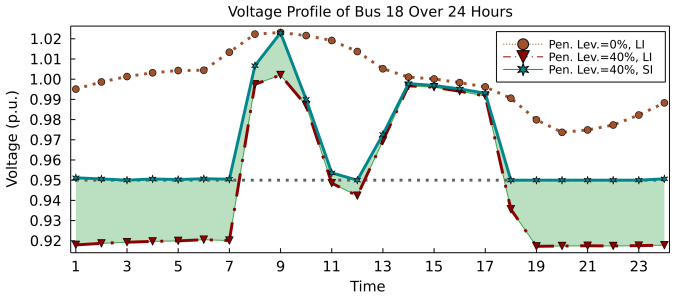

Fig. 5: Mitigating voltage violation using the proposed method

the desired range.The reactive power dispatch of *SI* of *EV* connected to bus 18 illustrated that the *SI* support the *DN* during the hours that voltage magnitude violation occurs as shown in Fig. 6. In Fig. 6, it should be noted that the positive sign for the real power of *SI* means that the *EV* is dispatching real power (i.e. V2G mode). It is an interesting observation that *SI*s increase the charging power of *EV*s in some hours and as a result increase V2G power in other hours. The *SI*s do this pattern to increase their ability to support the *DN*.

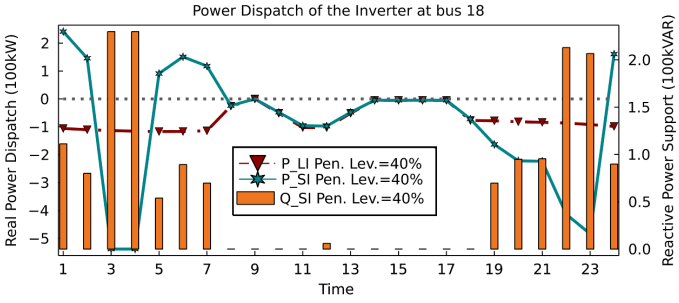

Fig. 6: Real and Reactive power dispatch of *EV*'s inverter

To present a fair comparison illustrating the merits of this work, the proposed *VVO* method with four quadrants *SI* (4Q-SI) is compared with the one with solar two quadrants *SI* (2Q-SI). With adding 4Q-SI to EVs, the operation cost of *DN* decreases from \$32,402 to \$29,775 and the *MFVM* index is decreased to 0 from 0.072.

The operation cost and the *MFVM* index of the *DN* is $\$31,509$ and 0.6, respectively when the *VVO* problem is formulated with linearized DC power flow along with a lossless model of *SI*s. In this case, the power flow equations are DC and the model of the *SI* connecting *DER*s to the *DN* is not accurate. The operation cost and the *MFVM* index of the *DN* procured by the proposed *VVO* problem in this paper with accurate *SI* model are $\$29,775$ and 0, respectively. Thus, utilizing the proposed *VVO* model decreases the voltage violations and the operation cost of the *DN*.

*2) **Impact of enabling V2G mode on the reactive power support of* **SI**s:* In this section, the impact of enabling V2G mode of *EV*s on the voltage profile support capability of *SI*s is investigated. Fig. 7 compares the voltage profile of bus 18 over 24 hours when V2G mode is enabled for *EV*s with the one procured when V2G mode is disabled. It should be noted that *EV*s penetration level is 40% for both scenarios. Enabling V2G mode mitigates the voltage magnitude violation by increasing the reactive power support of the *EV* as shown in Fig. 8.

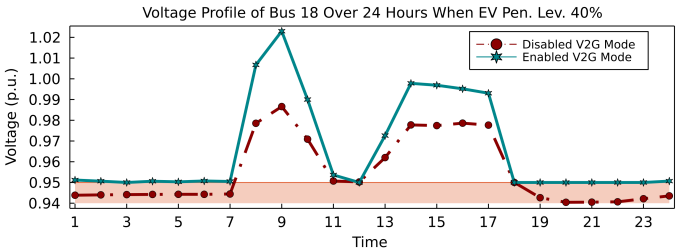

Fig. 7: Impact of enabling V2G mode on the voltage profile

Fig. 8 illustrates the real and reactive power dispatch of the *SI* connected to *EV* 17 (i.e., the *EV* connected to bus 18) for both scenarios. An interesting point is that the charging rate of *EV*s increases during the night hours since the reactive power support of *SI*s are increased. Thus, *EV*s minimize their cost by selling their energy in V2G mode and support the voltage profile of the network in the meantime by dispatching reactive power. Increasing the *AC* real power in charging and V2G modes increase the reactive power support of the *SI*s. Thus, increasing the charging power of *SI*s in those hours leads to the working of *EV*s in V2G mode in other night hours and that will lead to increasing the reactive power support of the *SI* in all night. The SI of the EV connected to bus 18 procured by the proposed *SI* model works in different power factors during 24 hours to support the reactive power as presented in Fig. 8.

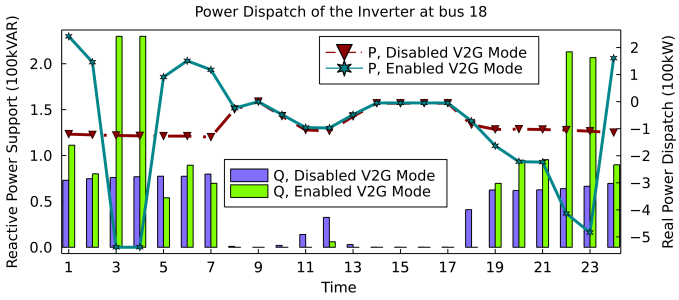

Fig. 8: Real and Reactive power dispatch of *EV*'s inverter

*3) **Impact of utilizing* **SI**s *on dispatchability of* **DER**s:* Utilizing high penetration level of *DER*s (such as solar generation units) might lead to generation curtailments within ADN. However, utilizing *SI*s can increases the dispatchability of renewable *DER*s. In this case, the penetration level of solar is increased to 80% and the penetration level of *EV*s is 10%. The curtailed solar power and reactive power dispatch of solar generation unit 4 which is connected to bus 7 are presented in Fig. 9. The curtailed solar dispatch of the network when LIs are utilized is 566.93 kWh over 24 hours. However, utilizing *SI*s cut the solar dispatch curtailment more than 51% to $277.56kWh$ over 24 hours.

Here, it is shown that utilizing *SI*s in the proposed *VVO* problem not only decreases the voltage magnitude violation but also enhances dispatchability of solar generation units. Fig. 10 illustrates how *SI*s increases the dispatchability of solar generation units by *decreasing the voltage magnitude*

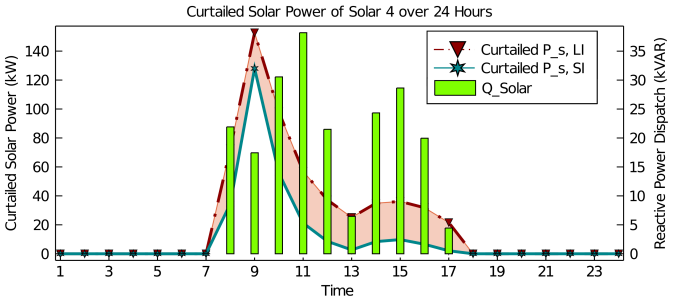

Fig. 9: Increasing the solar dispatchability by utilizing *SI*s

of buses experiencing over voltage. Note that in this case, the penetration level of solar generation units is 80%. *SI*s connected to the solar generation units exploit their grid service capacity to decrease the voltage magnitude violation and increase the dispatchability of solar generation units.

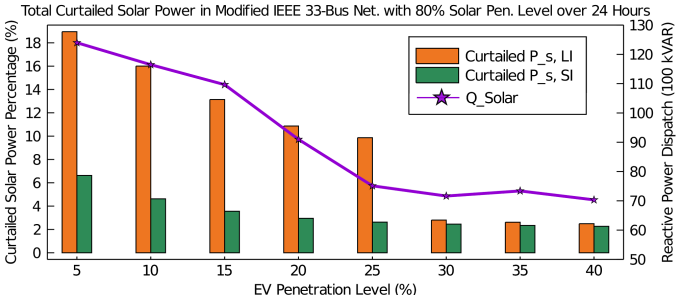

Fig. 10: The reduction in solar curtailment with *SI*

B. Modified IEEE 123-bus System

In this section, the modified IEEE 123-bus network is leveraged to illustrate the performance of the proposed method. An arbitrary configuration of the IEEE 123-bus system is selected in this part. The modified IEEE 123-bus system consists of 126 buses, 125 lines, 85 loads, 16 solar generation units, and 114 *EV*s as shown in Fig. 11. The green buses are the buses that *EV*s connected to them.

Fig. 12 illustrates how *SI*s mitigate the voltage magnitude violation in buses far from the feeder bus due to utilizing high penetration *EV*s. The voltage profile of the selected bus (i.e., bus 100) procured by the proposed *VVO* problem is compared with the one procured by the *VVO* problem with LIs in Fig. 12.A. To mitigate the voltage violation, the *SI*s change the charging power of *EV*s as shown in Fig. 12.B. to increase their capacity to support reactive power in those hours under voltage occurs as presented in Fig. 12.C. As presented in Fig. 11 solar generation unit 14 is connected to bus 100. Thus, the coordination between the *SI*s of *EV* and *PV* connected to bus 100 to decrease the voltage violation is presented in Fig. 12.C. Solar generation unit 14 utilizes its real power dispatch to support the grid by dispatching the reactive power to bus 100 as shown in Figs. 12.C and 12.D. The overall power quality of the *DN* increases when the proposed *SI* method is utilized. MFVM is used for the 123-bus system to compare the overall power quality of the *DN* procured by the proposed

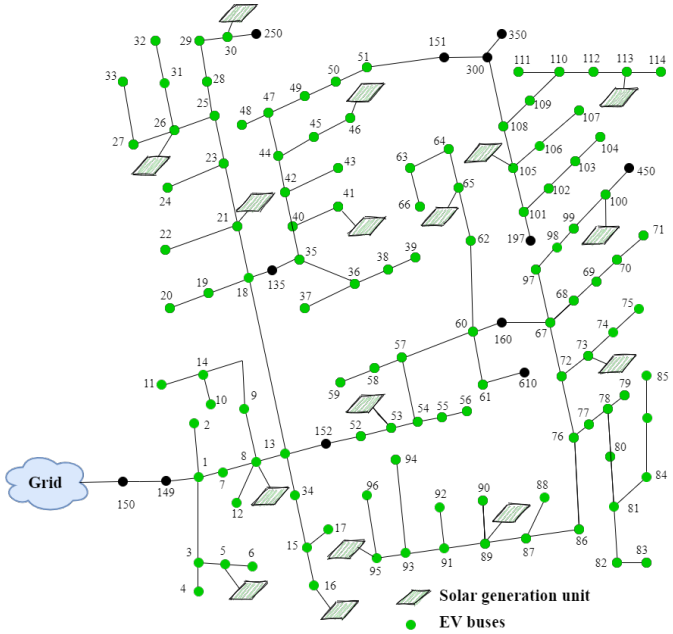

Fig. 11: The modified IEEE 123-bus *DN*

method with the one procured by the LI method. The MFVM index of the *DN* procured by the LI method is 0.037, and it is reduced by 97% to $1.2e^{-3}$ when the proposed method is utilized. Not only does the overall power quality increase when the proposed model is utilized but also the operation cost of the IEEE 123-bus system decreases by 1.6% from $\$479,980$ to $\$472,488$.

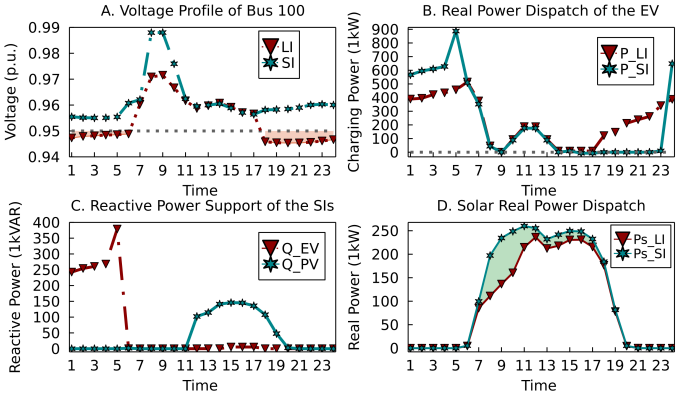

Fig. 12: Grid services of *SI*s

C. Three-Phase Unbalanced Case: Modified IEEE 123-bus System

In this section, the performance of the proposed VVO model with SIs is evaluated in a three-phase unbalanced distribution network. The mutual impedance of the three-phase line creates virtual loops in the graph structure of the network, resulting in a non-radial network. The SOCP relaxation method does not procure an exact solution for unbalanced three-phase distribution networks [55]. Hence, the two-stage algorithm presented in [56] is utilized to compare the proposed VVO model with the one with LIs.

The voltage magnitude of buses at 8 am as obtained by the proposed VVO problem with LI and with SI are presented in Figs. 13 and 14, respectively. The figures show that the use of SI brings the voltage profile of buses within the desired range (0.95 p.u. to 1.05 p.u.). The *SI* connecting *EVs* and solar generation units to the distribution network helps regulate the voltage profile of different phases of buses by dispatching reactive power to the network. The MFVM index of the *DN* procured by the *LI* case is $5e^{-3}$ for 40% *EV* penetration level and it is decreased to 0 when the proposed *SI* model is utilized. Besides, the operation cost procured by the *LI* model is $\$1.56M$, while the one procured by the *SI* model decreases by 3.2% to $\$1.51M$.

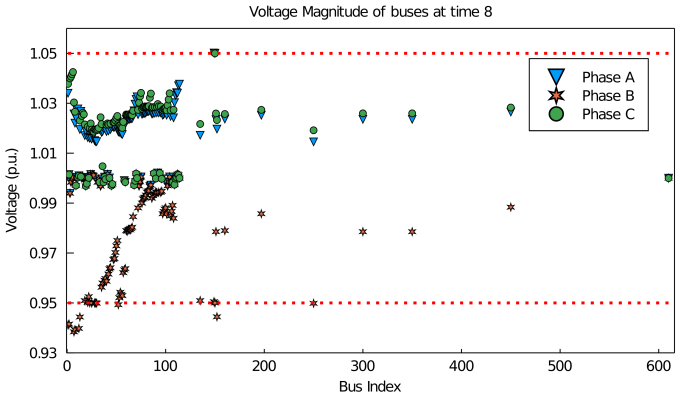

Fig. 13: The voltage profile of 123-bus system proposed by the *LI* model in under-voltage loading condition

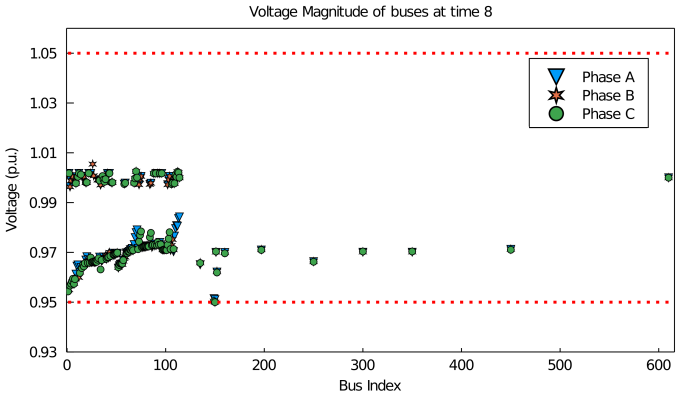

Fig. 14: The voltage profile of 123-bus system proposed by the proposed *SI* model in under-voltage loading condition

IV. Conclusion

This paper presented a *VVO* method for the *DN* in the presence of *EV* and *PV* systems. Utilizing *SI*s to connect *DER*s to the *DN* introduces grid service opportunities to the *DN*s. In this paper, the model of bidirectional *SI*s that can operate in different power factors is presented. Thus, the model of *DER*s (i.e., solar generation units and *EV*s in this paper) connected to these *SI*s in the *VVO* problem are presented. This problem is a non-convex optimization problem that is hard to solve. Thus, in this paper, the SOCP relaxation method is utilized to relax the bilinear terms in the power flow equations. Since the *DER*s connected to *SI*s might work in charging or discharging modes, the model of *DER*s connected to *SI*s based on the direction of their real and reactive power flow is proposed using a piece-wised linear P-Q characteristics model for *SI*s. The presented *VVO* method with *SI*s unleashes the grid services potential of *DER*s to increase the power quality in *DN*s. Also, the proposed *VVO* method increases the *DER*s dispatchability. However, the *SI*s utilize a portion of their input power to support the reactive power of *DN*s. Therefore, the operation cost of the *DN* will increase when *SI*s are utilized.

References

[1] I. T. Outlook, "Oecd publishing, paris," 2017.
[2] M. Wikström, L. Eriksson, and L. Hansson, "Introducing plug-in electric vehicles in public authorities," *Research in transportation business & management*, vol. 18, pp. 29–37, 2016.
[3] Z. Moghaddam, I. Ahmad, D. Habibi, and Q. V. Phung, "Smart charging strategy for electric vehicle charging stations," *IEEE Transactions on transportation electrification*, vol. 4, no. 1, pp. 76–88, 2017.
[4] A. Farokhi Soofi, R. Bayani, and S. D. Manshadi, "Analyzing power quality implications of high level charging rates of electric vehicle within distribution networks," in *2021 IEEE Transportation Electrification Conference & Expo (ITEC)*. IEEE, 2021, pp. 1–6.
[5] L. Lyu, X. Yang, Y. Xiang, J. Liu, S. Jawad, and R. Deng, "Exploring high-penetration electric vehicles impact on urban power grid based on voltage stability analysis," *Energy*, vol. 198, p. 117301, 2020.
[6] M. Farhoodnea, A. Mohamed, H. Shareef, and H. Zayandehroodi, "Power quality impacts of high-penetration electric vehicle stations and renewable energy-based generators on power distribution systems," *Measurement*, vol. 46, no. 8, pp. 2423–2434, 2013.
[7] Y. Yu, D. Reihs, S. Wagh, A. Shekhar, D. Stahleder, G. R. C. Mouli, F. Lehfuss, and P. Bauer, "Data-driven study of low voltage distribution grid behaviour with increasing electric vehicle penetration," *IEEE Access*, vol. 10, pp. 6053–6070, 2022.
[8] S. Deb, K. Kalita, and P. Mahanta, "Impact of electric vehicle charging stations on reliability of distribution network," in *2017 International Conference on Technological Advancements in Power and Energy (TAP Energy)*. IEEE, 2017, pp. 1–6.
[9] R.-C. Leou, C.-L. Su, and C.-N. Lu, "Stochastic analyses of electric vehicle charging impacts on distribution network," *IEEE Transactions on Power Systems*, vol. 29, no. 3, pp. 1055–1063, 2013.
[10] A. F. Soofi, R. Bayani, and S. D. Manshadi, "Investigating the impact of electric vehicles on the voltage profile of distribution networks," in *2022 IEEE Power & Energy Society Innovative Smart Grid Technologies Conference (ISGT)*. IEEE, 2022, pp. 1–5.
[11] C. B. Jones, W. Vining, M. Lave, T. Haines, C. Neuman, J. Bennett, and D. R. Scoffield, "Impact of electric vehicle customer response to time-of-use rates on distribution power grids," *Energy Reports*, vol. 8, pp. 8225–8235, 2022.
[12] Y. Zheng, S. Niu, Y. Shang, Z. Shao, and L. Jian, "Integrating plug-in electric vehicles into power grids: A comprehensive review on power interaction mode, scheduling methodology and mathematical foundation," *Renewable and Sustainable Energy Reviews*, vol. 112, pp. 424–439, 2019.
[13] C. Crozier, T. Morstyn, and M. McCulloch, "The opportunity for smart charging to mitigate the impact of electric vehicles on transmission and distribution systems," *Applied Energy*, vol. 268, p. 114973, 2020.
[14] O. Sadeghian, A. Oshnoei, B. Mohammadi-Ivatloo, V. Vahidinasab, and A. Anvari-Moghaddam, "A comprehensive review on electric vehicles smart charging: Solutions, strategies, technologies, and challenges," *Journal of Energy Storage*, vol. 54, p. 105241, 2022.
[15] J. García-Villalobos, I. Zamora, J. I. San Martín, F. J. Asensio, and V. Aperribay, "Plug-in electric vehicles in electric distribution networks: A review of smart charging approaches," *Renewable and Sustainable Energy Reviews*, vol. 38, pp. 717–731, 2014.
[16] A. J. Cheng, B. Tarroja, B. Shaffer, and S. Samuelsen, "Comparing the emissions benefits of centralized vs. decentralized electric vehicle smart charging approaches: A case study of the year 2030 california electric grid," *Journal of Power Sources*, vol. 401, pp. 175–185, 2018.
[17] J.-M. Clairand, J. Rodríguez-García, and C. Álvarez-Bel, "Smart charging for electric vehicle aggregators considering users' preferences," *IEEE Access*, vol. 6, pp. 54 624–54 635, 2018.

[18] M. Nour, S. M. Said, A. Ali, and C. Farkas, "Smart charging of electric vehicles according to electricity price," in *2019 International Conference on Innovative Trends in Computer Engineering (ITCE)*. IEEE, 2019, pp. 432–437.

[19] A. D. Hilshey, P. D. Hines, P. Rezaei, and J. R. Dowds, "Estimating the impact of electric vehicle smart charging on distribution transformer aging," *IEEE Transactions on Smart Grid*, vol. 4, no. 2, pp. 905–913, 2012.

[20] S. Rahman, I. A. Khan, A. A. Khan, A. Mallik, and M. F. Nadeem, "Comprehensive review & impact analysis of integrating projected electric vehicle charging load to the existing low voltage distribution system," *Renewable and Sustainable Energy Reviews*, vol. 153, p. 111756, 2022.

[21] S. Weckx, R. D'Hulst, B. Claessens, and J. Driesensam, "Multiagent charging of electric vehicles respecting distribution transformer loading and voltage limits," *IEEE Transactions on Smart Grid*, vol. 5, no. 6, pp. 2857–2867, 2014.

[22] L. Zhang, V. Kekatos, and G. B. Giannakis, "Scalable electric vehicle charging protocols," *IEEE Transactions on Power Systems*, vol. 32, no. 2, pp. 1451–1462, 2016.

[23] H. Ramadan, A. Ali, M. Nour, and C. Farkas, "Smart charging and discharging of plug-in electric vehicles for peak shaving and valley filling of the grid power," in *2018 Twentieth International Middle East Power Systems Conference (MEPCON)*. IEEE, 2018, pp. 735–739.

[24] H. Nafisi, S. M. M. Agah, H. A. Abyaneh, and M. Abedi, "Two-stage optimization method for energy loss minimization in microgrid based on smart power management scheme of phevs," *IEEE Transactions on Smart Grid*, vol. 7, no. 3, pp. 1268–1276, 2015.

[25] J.-M. Clairand, J. R. García, C. A. Bel, and P. P. Sarmiento, "A tariff system for electric vehicle smart charging to increase renewable energy sources use," in *2017 IEEE PES Innovative Smart Grid Technologies Conference-Latin America (ISGT Latin America)*. IEEE, 2017, pp. 1–6.

[26] Y. Dahmane, M. Ghanes, R. Chenouard, and M. Alvarado-Ruiz, "Decentralized control of electric vehicle smart charging for cost minimization considering temperature and battery health," in *2019 IEEE International Conference on Communications, Control, and Computing Technologies for Smart Grids (SmartGridComm)*. IEEE, 2019, pp. 1–6.

[27] G. Lacey, G. Putrus, and E. Bentley, "Smart ev charging schedules: supporting the grid and protecting battery life," *IET Electrical Systems in Transportation*, vol. 7, no. 1, pp. 84–91, 2017.

[28] M. H. Mobarak and J. Bauman, "Vehicle-directed smart charging strategies to mitigate the effect of long-range ev charging on distribution transformer aging," *IEEE Transactions on Transportation Electrification*, vol. 5, no. 4, pp. 1097–1111, 2019.

[29] J. Quirós-Tortós, L. F. Ochoa, S. W. Alnaser, and T. Butler, "Control of ev charging points for thermal and voltage management of lv networks," *IEEE Transactions on Power Systems*, vol. 31, no. 4, pp. 3028–3039, 2015.

[30] V. T. Tran, M. R. Islam, K. M. Muttaqi, and D. Sutanto, "A solar powered ev charging or discharging facility to support local power grids," in *2018 IEEE Industry Applications Society Annual Meeting (IAS)*. IEEE, 2018, pp. 1–7.

[31] F. Rahman and W. Xu, *Advances in solar photovoltaic power plants*. Springer, 2016.

[32] A. Woyte, V. Van Thong, R. Belmans, and J. Nijs, "Voltage fluctuations on distribution level introduced by photovoltaic systems," *IEEE Transactions on energy conversion*, vol. 21, no. 1, pp. 202–209, 2006.

[33] S. A. Abdelrazek and S. Kamalasadan, "Integrated pv capacity firming and energy time shift battery energy storage management using energy-oriented optimization," *IEEE Transactions on Industry Applications*, vol. 52, no. 3, pp. 2607–2617, 2016.

[34] S. Sikkabut, P. Mungporn, C. Ekkaravarodome, N. Bizon, P. Tricoli, B. Nahid-Mobarakeh, S. Pierfederici, B. Davat, and P. Thounthong, "Control of high-energy high-power densities storage devices by li-ion battery and supercapacitor for fuel cell/photovoltaic hybrid power plant for autonomous system applications," *IEEE Transactions on Industry Applications*, vol. 52, no. 5, pp. 4395–4407, 2016.

[35] S. Barcellona, L. Piegari, V. Musolino, and C. Ballif, "Economic viability for residential battery storage systems in grid-connected pv plants," *IET Renewable Power Generation*, vol. 12, no. 2, pp. 135–142, 2018.

[36] M. J. E. Alam, K. M. Muttaqi, and D. Sutanto, "Effective utilization of available pev battery capacity for mitigation of solar pv impact and grid support with integrated v2g functionality," *IEEE Transactions on Smart Grid*, vol. 7, no. 3, pp. 1562–1571, 2015.

[37] N. Saxena, I. Hussain, B. Singh, and A. L. Vyas, "Implementation of a grid-integrated pv-battery system for residential and electrical vehicle applications," *IEEE Transactions on Industrial Electronics*, vol. 65, no. 8, pp. 6592–6601, 2017.

[38] V. T. Tran, M. R. Islam, K. M. Muttaqi, and D. Sutanto, "An efficient energy management approach for a solar-powered ev battery charging facility to support distribution grids," *IEEE Transactions on Industry Applications*, vol. 55, no. 6, pp. 6517–6526, 2019.

[39] M. M. Biswas, S. R. Akhter, and K. C. Paul, "Power quality analysis for distributed generation and electric vehicle integrated distribution system," in *2020 55th International Universities Power Engineering Conference (UPEC)*. IEEE, 2020, pp. 1–6.

[40] A. H. Zaidi, K. Sunderland, and M. Conlon, "Role of reactive power (statcom) in the planning of distribution network with higher ev charging level," *IET Generation, Transmission & Distribution*, vol. 13, no. 7, pp. 951–959, 2019.

[41] J. Smith, W. Sunderman, R. Dugan, and B. Seal, "Smart inverter volt/var control functions for high penetration of pv on distribution systems," in *2011 IEEE/PES Power Systems Conference and Exposition*. IEEE, 2011, pp. 1–6.

[42] M. H. K. Tushar and C. Assi, "Volt-var control through joint optimization of capacitor bank switching, renewable energy, and home appliances," *IEEE transactions on smart grid*, vol. 9, no. 5, pp. 4077–4086, 2017.

[43] H. Abdullah, R. M. Kamel, and A. Gastli, "Ev impact on the residential distribution network with smart pv inverters," in *2020 IEEE Power & Energy Society Innovative Smart Grid Technologies Conference (ISGT)*. IEEE, 2020, pp. 1–6.

[44] X. Su, M. A. Masoum, and P. J. Wolfs, "Optimal pv inverter reactive power control and real power curtailment to improve performance of unbalanced four-wire lv distribution networks," *IEEE Transactions on Sustainable Energy*, vol. 5, no. 3, pp. 967–977, 2014.

[45] R. R. Jha, A. Dubey, C.-C. Liu, and K. P. Schneider, "Bi-level volt-var optimization to coordinate smart inverters with voltage control devices," *IEEE Transactions on Power Systems*, vol. 34, no. 3, pp. 1801–1813, 2019.

[46] T. M. Aljohani, A. Saad, and O. A. Mohammed, "Two-stage optimization strategy for solving the vvo problem considering high penetration of plug-in electric vehicles to unbalanced distribution networks," *IEEE Transactions on Industry Applications*, vol. 57, no. 4, pp. 3425–3440, 2021.

[47] B. Kocuk, S. S. Dey, and X. A. Sun, "Strong socp relaxations for the optimal power flow problem," *Operations Research*, vol. 64, no. 6, pp. 1177–1196, 2016.

[48] A. Farokhi-Soofi, S. D. Manshadi, G. Liu, and R. Dai, "A socp relaxation for cycle constraints in the optimal power flow problem," *IEEE Transactions on Smart Grid*, vol. 99, no. 4, pp. 1–10, 2020.

[49] K.-N. D. Malamaki and C. S. Demoulias, "Estimation of additional pv converter losses operating under pf$\neq$ 1 based on manufacturer's data at pf= 1," *IEEE Transactions on Energy Conversion*, vol. 34, no. 1, pp. 540–553, 2019.

[50] A. Farokhi-Soofi and S. D. Manshadi, "Demand variation impact on tightness of convex relaxation approaches for the acopf problem," in *2020 52nd North American Power Symposium (NAPS)*. IEEE, 2021, pp. 1–6.

[51] S. H. Low, "Convex relaxation of optimal power flow—part ii: Exactness," *IEEE Transactions on Control of Network Systems*, vol. 1, no. 2, pp. 177–189, 2014.

[52] R. R. Jha, A. Inaolaji, B. D. Biswas, A. Suresh, A. Dubey, S. Paudyal, and S. Kamalasadan, "Distribution grid optimal power flow (d-opf): Modeling, analysis, and benchmarking," *IEEE Transactions on Power Systems*, 2022.

[53] L. Gurobi Optimization, "Gurobi optimizer reference manual," 2020.

[54] "Caiso — california iso," https://www.caiso.com/Pages/default.aspx, (Accessed on 11/03/2021).

[55] N. Nazir, P. Racherla, and M. Almassalkhi, "Optimal multi-period dispatch of distributed energy resources in unbalanced distribution feeders," *IEEE Transactions on Power Systems*, vol. 35, no. 4, pp. 2683–2692, 2020.

[56] M. He, Z. Soltani, M. Ghaljehei, M. Esmaili, S. Ma, M. Chen, M. Khorsand, R. Ayyanar, and V. Vittal, "A socp-based acopf for operational scheduling of three-phase unbalanced distribution systems and coordination of pv smart inverters," *IEEE Transactions on Power Systems*, 2023.

Arash Farokhi Soofi (S'14) received the B.S. and M.S. degrees in electrical power engineering from the Amirkabir University of Technology, Tehran, Iran, in 2015 and 2018, respectively. He is currently pursuing a Ph.D. degree in electrical engineering from the Department of Electrical and Computer Engineering, San Diego State University and University of California San Diego, San Diego, CA, USA. His current research interests include convex relaxation, bi-level optimization, and power system operation and planning.

Saeed D. Manshadi (M'18) received a B.S. degree from the University of Tehran, Tehran, Iran, in 2012, the M.S. degree from the University at Buffalo, State University of New York, Buffalo, NY, USA, in 2014, and the Ph.D. degree from Southern Methodist University, Dallas, TX, USA, in 2018, all in electrical engineering. He was a Postdoctoral Fellow with the University of California, Riverside, CA, USA. He is currently an Assistant Professor with the Department of Electrical and Computer Engineering, San Diego State University, San Diego, CA, USA. His research interests include smart grids, microgrids, integrating renewable and distributed resources, and power system operation and planning. Dr. Manshadi is an Associate Editor of the IEEE TRANSACTIONS ON VEHICULAR TECHNOLOGY.